J MATER RES TECHNOL. 2019;8(4):3603–3611

Available online at www.sciencedirect.com

jmr&t Journal of Materials Research and Technology

www.jmrt.com.br

Original Article

Bridging the local configurations and crystalline counterparts of bulk metallic glass by nanocalorimetry

Bingge Zhao[a,b], *Bin Yang*[c], *Javier Rodríguez-Viejo*[d], *Mannan Wu*[a], *Christoph Schick*[c,e], *Qijie Zhai*[a], *Yulai Gao*[a,b,*]

[a] *Center for Advanced Solidification Technology (CAST), School of Materials Science and Engineering, Shanghai University, 99 Shangda Road, 200444 Shanghai, PR China*

[b] *Laboratory for Microstructures, Institute of Materials, Shanghai University, 99 Shangda Road, 200444 Shanghai, PR China*

[c] *Institute of Physics and Competence Centre CALOR, University of Rostock, Albert-Einstein-Street 23-24, Rostock 18051, Germany*

[d] *Physics Department, Universitat Autònoma de Barcelona, Bellaterra 08193, Spain*

[e] *Kazan Federal University, 18 Kremlyovskaya Street, Kazan 420008, Russian Federation*

ARTICLE INFO

Article history:
Received 19 December 2018
Accepted 30 May 2019
Available online 10 June 2019

Keywords:
Nanocalorimetry
Nucleation
Crystal growth
Metallic glass
Quasicrystal

ABSTRACT

The structural understanding of crystallization in bulk metallic glasses (BMGs) has attracted much attention while rapid crystallization occurring under controllable conditions is less involved. In this study, a $Ce_{68}Al_{10}Cu_{20}Co_2$ (at.%) BMG was thermally devitrified by differential scanning calorimetry (DSC) and nanocalorimetry. At a heating rate of 10 K/min by DSC, $AlCe_3$ and Ce are the major crystalline phases after devitrification while $Al_{13}Co_4$ quasicrystals and Ce are the dominant phases in the crystallization products at a heating rate of 5000 K/s by nanocalorimetry. Attributing to the covalent-like bond in Al–Co atom pairs, $Al_{13}Co_4$ quasicrystals precipitate in the primary crystallization and work as the precursors associating local atomic configurations in the glassy state with crystalline phases after crystallization. Attributing to the enhanced mobility of Cu atoms, compositional redistribution occurs in the as-cast sample. On nanocalorimetry heating, an unambiguous discrepancy in the nucleation and growth of the nano-sized $Al_{13}Co_4$ quasicrystals is thus triggered, contributing to an obvious difference in the crystal size. This research unveils the distinct crystallization behaviors of Ce-based BMG on rapid heating. The formation of quasicrystals demonstrates the multi-stage crystallization on rapid heating and bridges the structural gap between local atomic configurations of metallic glasses and crystalline phases.

1. Introduction

Since the first preparation of bulk metallic glasses (BMGs) by Duwez [1], tremendous attention from both the fundamental and practical disciplines has been paid to this area attributing to their intriguing structural and mechanical

* *Corresponding author.*
E-mail: ylgao@shu.edu.cn (Y. Gao).

https://doi.org/10.1016/j.jmrt.2019.05.023

properties [2–5]. According to the classical nucleation theory (CNT), atom motions slow down and enthalpy decreases rapidly upon quenching the metallic melt below its melting temperature. With different undercooling, various nucleation and growth behaviors are expected, changing the final structure and mechanical properties [6–11]. If crystallization on cooling is totally suppressed, the undercooled liquid falls out of equilibrium, and therefore an amorphous state is preserved. Compared with crystalline phases, an excess Gibbs free energy is trapped in the metallic glass. Driven by such excess energy, BMG undergoes glass transition and crystallization at elevated temperatures. Up to now, the kinetics and structure evolution on crystallization in various BMGs have been synthetically demonstrated by thermal analysis and structural characterization [12,13]. However, most of these studies were performed under near-equilibrium conditions. For example, the heating rates of the conventional differential scanning calorimetry (DSC) are usually centered at tens of K/min [14]. In view of the pronounced relationship between solidification behavior and cooling rate [15], it is extremely attractive to comparatively figure out what is able to happen on rapid heating. However, due to the deficiency of conventional DSC, a novel calorimetry that can provide enhanced heating capability is vigorously needed. With the development of microelectromechanical systems (MEMS) technology, nanocalorimetry, which was initially designed by Allen and Hellman et al., provides a solution to this problem attributing to its ultrafast heating rate as high as 10^6 K/s [16,17]. Furthermore, the sensitivity of nanocalorimetry is substantially improved, making it capable of capturing weak thermal signals and revealing phase transitions in nanoscale systems [18–20]. On rapid heating, it has been demonstrated that both crystallization kinetics and structure evolutions are possible to change. For example, a curved Kissinger plot depicting the crystallization kinetics of $Ge_2Sb_2Te_5$ (at.%) was obtained by Greer, confirming the growth-controlled crystallization on heating and a decoupling between crystal growth and viscous flow in the deeply undercooled liquid [21]. This phenomenon is deemed to occur in many other fragile phase-change materials (PCMs) [22,23]. In terms of metallic glasses, Vlassak introduced the nanocalorimetry to the rapid crystallization of $Cu_{50}Zr_{50}$ (at.%) thin films, where the decoupling and crystallization asymmetry on heating and cooling were demonstrated as well [24]. Yang further identified the decoupling temperature in an Al-based metallic glass by heating at rates spanning over six orders of magnitude [25]. With the help of nanocalorimetry, our previous studies realized in situ preparation of metallic glass and made it possible to tune the microstructure of metallic glass, and the structural effect in determining the crystallization behaviors were revealed [26,27]. Another remarkable issue about the rapid crystallization by nanocalorimetry is the structure evolution. Some equilibrium phases can be suppressed while some other new metastable phases can form under extreme non-equilibrium condition [28–30]. If the heating rate is further increased, crystallization may be totally suppressed [9,31]. Based on those scientific outcomes, it is expected that nanocalorimetry opens new avenues to rapid crystallization under extreme conditions.

Differential fast scanning calorimetry (DFSC), a nanocalorimetric instrument designed by Schick [32], achieves in situ heating and quenching at rates up to 10^5 K/s, and it has been widely employed to reveal the rapid phase transitions of metals [20,26,27,33–36]. Although high-temperature DFSC sensor became available recently [25], alloys with low crystallization temperature are still preferred to guarantee the full crystallization in studying the rapid crystallization of bulk metallic glasses. Ce-based BMG is deemed as an ideal candidate because of its high glass forming ability (GFA), low crystallization temperature, and good stability [37–39]. In this paper, $Ce_{68}Al_{10}Cu_{20}Co_2$ (at.%) BMG samples were crystallized by DSC and DFSC respectively, revealing that the crystallization products are evidently affected by heating rate. On DSC heating at 10 K/min, Ce and $AlCe_3$ with a small fraction of Al_5Co_2 were detected after crystallization. Whereas at the heating rate of 5000 K/s by DFSC, $Al_{13}Co_4$ with the quasicrystalline structure, which precipitates in the early stage of crystallization, was captured. Based on the diffusion of Co under these two conditions, the whole crystallization trajectory was depicted. According to the atom pairs in this BMG and Gibbs free energy in Al–Co binary system, the role of Co element in the formation and evolution of Al–Co intermetallic compounds was determined. As a result, primary and secondary crystallization were proposed during the rapid devitrification of $Ce_{68}Al_{10}Cu_{20}Co_2$ BMG. Cu atoms, on the other hand, have higher mobility and can diffuse even at room temperature, leading to a composition fluctuation in the as-cast sample. Both the nucleation and growth of $Al_{13}Co_4$ quasicrystals on following heating are influenced by the diffusion of Cu, causing the discrepancy in quasicrystal sizes.

2. Methods

$Ce_{68}Al_{10}Cu_{20}Co_2$ (at.%) master alloy was prepared by arc melting pure Ce, Al, Cu and Co in high-purity argon atmosphere. The purity of Ce is about 99.5 wt.% while other metals have purity at least 99.9 wt.%. Then the ingot was melted and quenched by suction casting to get a cylindrical rod with a diameter of 3 mm. The amorphous structure was examined by X-ray diffraction (XRD, D/Max-2200, Rigaku) with Cu K_α radiation ($\lambda = 0.154056$ nm) at a scanning rate of 4°/min. High-resolution transmission electron microscopy (HRTEM, JEM-2010F, JEOL) was used to further certify the amorphous structure. Using plastic abrasive paper, micro-sized samples were ground from the as-cast rod and then loaded onto a copper mesh. The wedge-shaped edge of these samples is sufficiently thin for HRTEM observation. Glass transition temperature (T_g), crystallization temperature (T_x) and melting temperature (T_m) were determined by DSC (Diamond, PerkinElmer Instruments) at heating rates of 5, 10, 20, 40, and 80 K/min.

To identify crystallization products, one BMG sample was fully crystallized by heating it from 323 K to 573 K (before T_m, without melting) at 10 K/min using DSC, which was immediately followed by free cooling. Crystallization products were then examined by XRD at a scanning rate of 4°/min.

As for DFSC measurement, XI 39395 sensor (Xensor Integration, Netherlands) with a measuring area of 60 μm × 70 μm

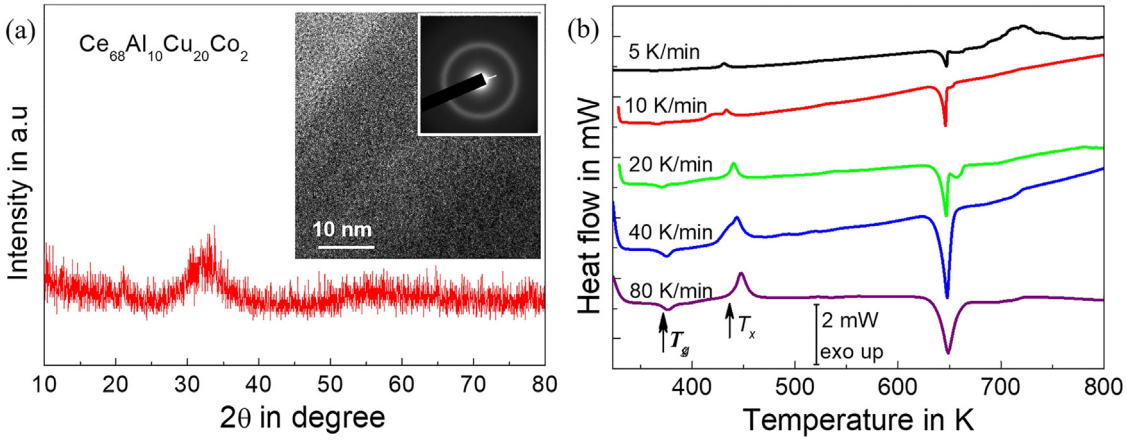

Fig. 1 – Characterization on the as-cast sample. (a) XRD pattern of the as-cast $Ce_{68}Al_{10}Cu_{20}Co_2$ rod. The broad peak indicates the glassy nature of the sample. Insets are HRTEM image and corresponding SAED pattern, further indicating the amorphous state. (b) DSC curves of the as-cast samples. A dominating endothermic peak rather than the glass transition step is detected because of the enthalpy rejuvenation.

was used. A small amount of silicon oil was spread on the sensor to improve the thermal contact between sample and membrane. Micro-sized samples were cut from the as-cast rod. A sample having an estimated size of 20 μm was picked up using a copper wire and then positioned in the center of the measuring area with the help of optical microscopy (Stemi 2000, Carl Zeiss). Then it was heated from 320 K to 621 K to get full crystallization without melting, which was followed by quenching at 5000 K/s down to room temperature. After quenching, this crystallized sample was thinned by focused ion beam (FIB, Helios NanoLab 600i, FEI). Its morphology, structure and composition were then characterized by HRTEM equipped with energy dispersive spectroscopy (EDS, Oxford). For comparison, another as-cast sample was machined by FIB and characterized by HRTEM to show the structure after casting. In addition to the TEM bright-field images, high angle annular dark field-scanning transmission electron microscopy (HAADF-STEM) images were captured to distinguish the composition fluctuation both in the as-cast and as-crystallized sample.

3. Results and discussion

The absence of sharp diffraction peaks in the XRD pattern (Fig. 1a) confirms the amorphous nature of the as-cast $Ce_{68}Al_{10}Cu_{20}Co_2$ sample. HRTEM image and selected area electron diffraction (SAED) pattern further verify the amorphous state. Fig. 1b represents DSC heating curves at different rates. Both glass transition and sharp crystallization peak are observed, confirming the XRD and HRTEM results in Fig. 1a. T_g, T_x and T_m are 358 K, 430 K and 641 K respectively at the heating rate of 5 K/min. They are considered as the reference temperatures for the following calorimetric measurements. Using Kissinger model, the activation energy of crystallization ($E_{a,c}$) is estimated as 239.4 kJ/mol. This large value suggests that $Ce_{68}Al_{10}Cu_{20}Co_2$ has a higher thermal stability against crystallization in Ce-based metallic glasses, agreeing with its higher glass forming ability than those CeAlCu BMGs [38,40].

For $Ce_{68}Al_{10}Cu_{20}Co_2$ BMG, its T_g is close to room temperature, and enthalpy relaxation is possible to occur even just after suction casting. When the as-cast sample is heated, the relaxed enthalpy rejuvenates, and an endothermic peak rather than a step change is detected at the glass transition, as indicated in Fig. 1b.

By DSC heating from 320 K to 621 K at 10 K/min, the as-cast sample was fully crystallized. Both the DSC curve and corresponding XRD pattern are shown in Fig. 2. The dominant phases are Ce and $AlCe_3$, which agrees well with the results in Ref. [41]. In addition, Al_5Co_2 is identified here after the crystallization by DSC. According to the Scherrer equation [42], the mean size of the crystals is roughly estimated to be 19 nm.

The lower heating rate by DSC guarantees the full crystallization while DFSC can expose the initial crystallization stage by the ultrafast heating rate. Fig. 3a shows the DFSC heating curve at 5000 K/s. In contrast to the DSC traces in Fig. 1b, two endothermic peaks near T_g are detected in the

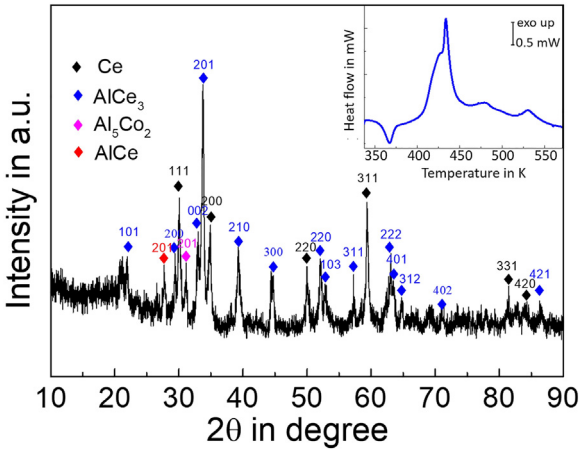

Fig. 2 – XRD pattern of $Ce_{68}Al_{10}Cu_{20}Co_2$ sample after heating at 10 K/min. $AlCe_3$ and Ce are the principal crystals. The inset shows the DSC heating curve for full crystallization.

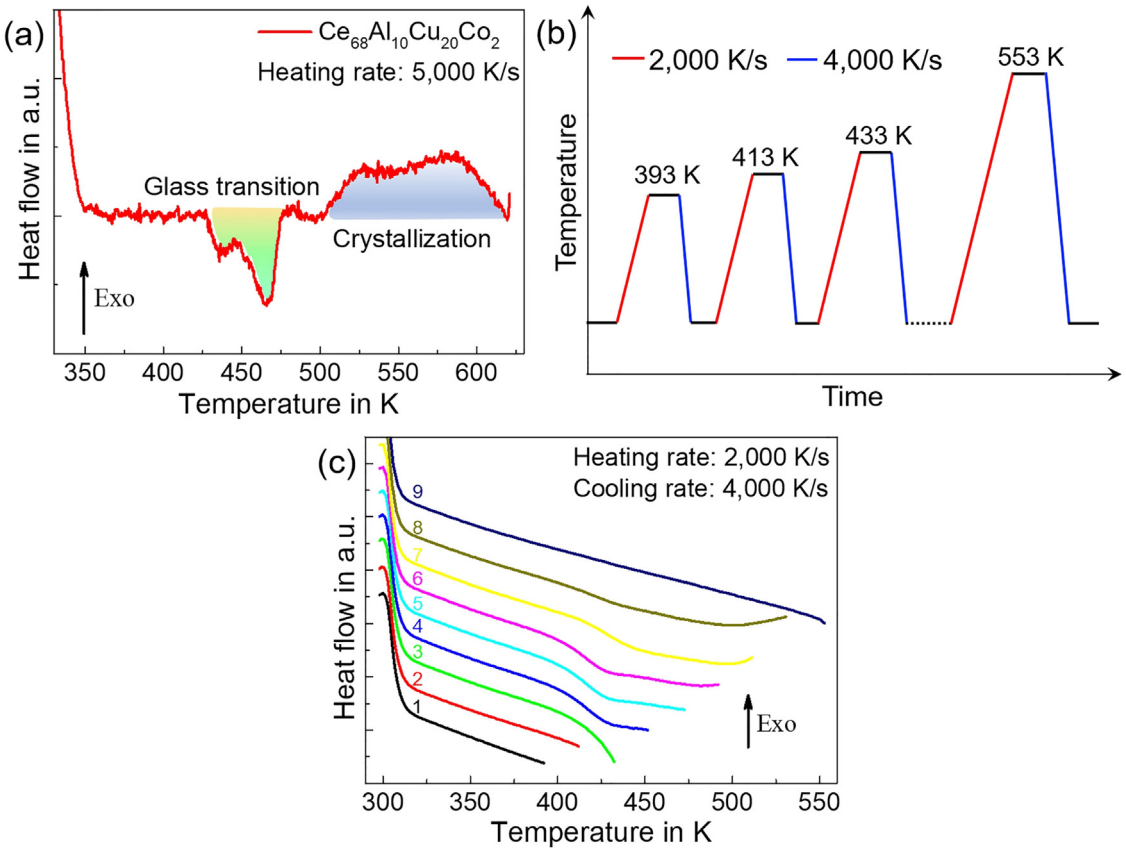

Fig. 3 – Nanocalorimetry curves indicating the glass transition and crystallization of the as-cast sample. (a) DFSC heating curve at 5000 K/s. The glass transition and crystallization are patterned in green and blue respectively. (b) Temperature profile for step scanning. The temperature step between two cycles is 20 K with heating and cooling rates of 2000 K/s and 4000 K/s, respectively. (c) Heating curves of the step scanning on one sample. When the sample is scanned below T_g (Curves 1 and 2), there are no visible phase transitions. One reversible endothermic step corresponding to glass transition is detected when the sample is scanned between amorphous solid and undercooled liquid. Since the thermal history can be erased at temperature higher than T_g, the double glass transition in the as-cast sample is associated with room-temperature aging and corresponding structural heterogeneity caused by atom rearrangement. (For interpretation of the references to color in this figure legend, the reader is referred to the web version of this article.)

DFSC heating curve. To exclude the effect of silicone oil, similar amount of silicone oil was spread on the sensor and was scanned using the same nanocalorimetric profile. No peaks corresponding to phase transitions of silicone oil are detected (Fig. S1), suggesting that the distinct behavior of glass transition and crystallization in DFSC measurement comes from $Ce_{68}Al_{10}Cu_{20}Co_2$. In addition, analogous results are observed in the nanocalorimetric measurement at 1000 K/s and 10,000 K/s (Fig. S2). A step scanning was performed on another sample to determine the dual endothermic peaks. The temperature profile is displayed in Fig. 3b: the sample is heated at 2000 K/s from room temperature to 393 K. After holding for 0.06 s, it is quenched down to room temperature at 4000 K/s. Then the cycle with temperature step of 20 K is repeated until the final temperature reaches 553 K. The results are shown in Fig. 3c. When the sample is cycled below T_g, there are no obvious peaks (Curves 1 and 2). But as the maximum temperature on heating is above T_g (Curves 3–7), an endothermic step rather than dual peaks is repeatedly observed, which is the reversible characteristic of glass transition [43]. It is noteworthy that the thermal history including structure relaxation can be erased when the metallic glass is heated to enter the undercooled liquid region. If the phase separation occurs in the as-cast sample, the double glass transition should always appear in the cycles without crystallization, which disagrees with the nanocalorimetry curves shown in Fig. 3b. This contradictory case implies that the dual peaks in glass transition are related to the structure heterogeneity formed during the room-temperature aging after the suction casting of the alloy, and its mechanism will be discussed later in this paper. The absence of the dual endothermic peaks in the DSC curves may be due to the limited sensitivity of this conventional calorimetric method. As the temperature increases further (Curve 8), an exothermic event associated with the crystallization of the undercooled liquid is detected. The next reheating curve (Curve 9) shows no traces of a glass transition, indicating the crystalline nature of the sample before the temperature scan. The overall crystallization process consists of two exothermic peaks, which will be demonstrated based on the structure characterization.

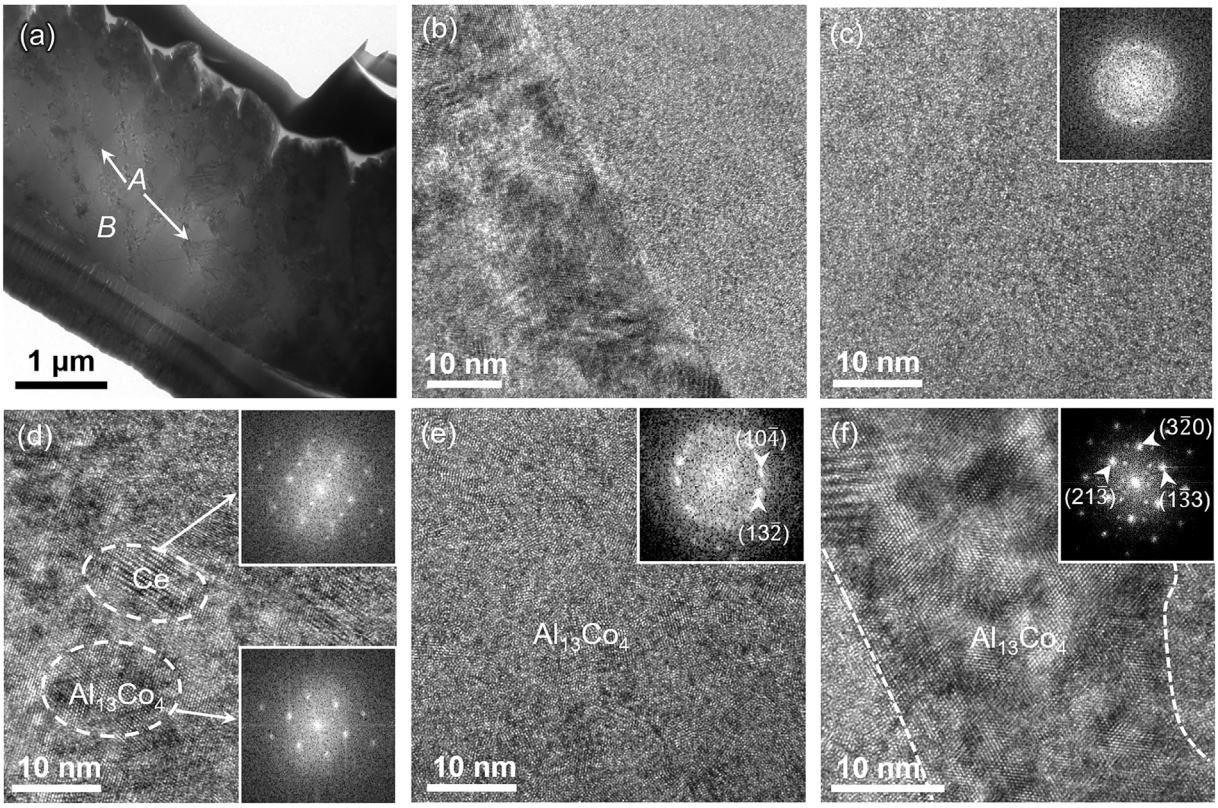

Fig. 4 – Structure characterization on $Ce_{68}Al_{10}Cu_{20}Co_2$ after rapid crystallization by DFSC. (a) The bright-field TEM image showing the bright (A) and dark (B) contrasts in the sample. The contrast suggests the different crystallographic orientations. (b) HRTEM image showing the interface between area A and B. Apparent size variations are observed. (c) The residual amorphous phase after rapid crystallization. (d) HRTEM image showing Ce and $Al_{13}Co_4$. They are the main ordered phases after rapid crystallization. (e and f) The HRTEM images corresponding to region A and B respectively. $Al_{13}Co_4$ are confirmed in both regions with an obvious size variation. Insets are the FFT patterns corresponding to the HRTEM image.

TEM bright-field images of the sample that was crystallized at 5000 K/s are displayed in Fig. 4. Regions with different contrasts, marked as *A* and *B* respectively, are clearly distinguished (Fig. 4a), indicating variations in crystallographic orientations after rapid crystallization. In the high-resolution images, both regions contain a large number of nanocrystals of different sizes, as displayed in Fig. 4b. In area *A*, most of the crystals are less than 5 nm while in area *B*, the crystals are several tens of nanometers. These nanocrystals suggest an extremely high nucleation rate but a slow growth velocity during crystallization, agreeing well with the growth-limited crystallization on heating [9,24]. As mentioned above, the mean size of the crystals after DSC heating is about 19 nm, not far from those measured after fast heating. In contrast, Tkatch found a reduction of crystal size from 320 nm to 48 nm as the heating rate increased from 10 K/min to 10^4 K/s in FeB metallic glass [44]. While in the CuZrAl bulk metallic glass, the crystalline phase produced at 250 K/s is about 1.5 μm which is two times smaller than that obtained at 750 K/s [45]. These two studies contradict current results, implying the crystallization of $Ce_{68}Al_{10}Cu_{20}Co_2$ is insensitive to the heating rate. Based on Farjas's research [46], crystal size on crystallization is essentially dependent on the ratio between activation energies of nucleation and growth rather than external experimental conditions, and that is why a comparison between nucleation rate and growth velocity is important [47]. To determine the relationship between crystal size and heating rate experimentally, further explorations are still needed. Apart from the ordered phases, a few amorphous phases were still retained after rapid crystallization (Fig. 4c). Theoretically, crystallization can be suppressed by ultrahigh heating rate, where amorphous structure can survive up to the melting point [48,49]. Experimentally, this has been verified in $Zr_{41}Ti_{14}Cu_{12}Ni_{10}Be_{23}$ (at.%) and $Au_{49}Ag_{5.5}Pd_{2.3}Cu_{26.9}Si_{16.3}$ (at.%) metallic glasses [6,9]. This scenario of the mixed crystalline-glassy structure highlights the crucial role of crystal growth in the formation of amorphous structure, as stated by Greer [5]. In current case, ordered clusters nucleate on previous cooling (suction casting). Then they grow on fast heating, where the growth rate is too sluggish to crystallize the whole sample, leaving the residual amorphous phase between different grains. This can be further demonstrated by the nano-sized crystals in Fig. 4.

By the fast Fourier transform (FFT) patterns, the ordered phases observed in Fig. 4d are consistent with Ce (ICDD-JCPDS card No. 65-3368) and $Al_{13}Co_4$ (ICDD-JCPDS card No. 65-1165) respectively. This result differs from the crystallization products at 10 K/min (Fig. 2). Furthermore, it is interesting to note

that $Al_{13}Co_4$ possesses an orthorhombic structure belonging to *Pmn*21 space group, and this phase has been confirmed as a quasicrystal [50,51]. Since $Al_{13}Co_4$ phase exhibits 10-fold symmetry in (1 0 0) plane [50], the typical diffraction pattern of a quasicrystal is not recognized in the FFT pattern (Fig. 4e and f). The formation of $Al_{13}Co_4$ quasicrystals can be illustrated as follows. In CeAlCuCo BMGs, Al-centered icosahedrons, which presumably form on quenching, are the predominant structural building blocks which constitute the essential units [52]. These local units are far below the critical size of a nucleus and cannot work as the heterogeneous sites like macroscopic impurities. As recognized, nucleation barrier arises from the difference between local structure of the undercooled liquid and the ordered crystals. Compared with a crystalline phase, there is a significant structural similarity between local icosahedron configurations and quasicrystalline phases. Although these local icosahedrons are very small, a decreased surface energy and nucleation barrier are generated [53], facilitating the formation of quasicrystals. This argument agrees with the consideration that the topographical short-range order dominates the nucleation of quasicrystals [54]. It has been demonstrated that the *sp* electrons of Al atoms can hybridize with the 3*d* electrons of late transition metals (such as Co, Ni, Fe) [38], which shortens the bond length and produces the covalent-like bond. According to Holland-Moritz's study, the bond length of Al–Co is only 2.535 Å [54] which is smaller than Al–Cu (2.74 Å) and Al–Ce bond (3.356 Å) [55]. This situation suggests a high priority to form Al–Co compounds during the crystallization of $Ce_{68}Al_{10}Cu_{20}Co_2$. According to Al–Co binary phase diagram [56], there are several kinds of Al–Co intermetallic compounds. Based on Sudavtsova's study [57], Fig. 5 schematically plots the dependence of Gibbs free energy on Co content at the onset temperature of crystallization (500 K). In the light of the thermodynamics, Al_5Co_2, a stable phase, should precipitate from the amorphous matrix because of its lower Gibbs free energy. However, in contrast to Al_5Co_2 crystals with hexagonal structure, $Al_{13}Co_4$ is a quasicrystalline phase that is structurally similar with the local atomic configurations units of the metallic glass. As mentioned above, it is the decreased nucleation barrier resulting from the structural similarity that contributes to the precipitation of $Al_{13}Co_4$ rather than Al_5Co_2. Following the nucleation, quasicrystal growth occurs on heating, in which the diffusion of Co is considered as the essential factor. As indicated by the free energy change in Fig. 5, metastable $Al_{13}Co_4$ quasicrystals evolve to stable crystalline Al_5Co_2 phases with a sufficient diffusion of Co at elevated temperatures. In summary, $Al_{13}Co_4$ quasicrystals can overcome the energy barrier and precipitate as the intermediate phase between local icosahedron structure and equilibrium crystals, which corresponds to the statement on evolution of quasicrystals.

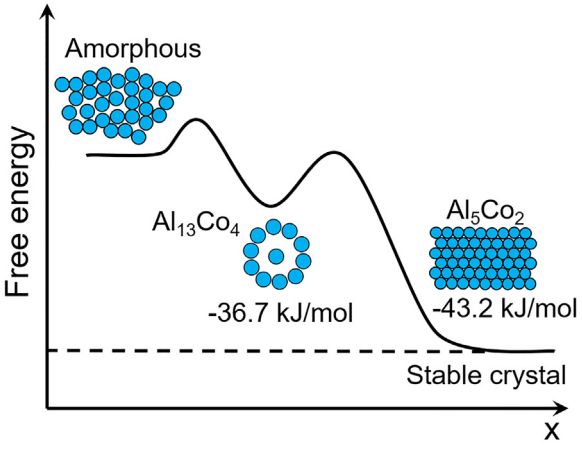

Fig. 5 – Schematic depicting the evolution of Gibbs free energy versus reaction coordinate on crystallization. $Al_{13}Co_4$ quasicrystals preferentially precipitate attributing to their structural similarity with Al-centered icosahedron in BMG although Al_5Co_2 is more thermodynamically stable. At elevated temperatures, metastable quasicrystals react with undercooled liquid to form stable crystals. The free energy of $Al_{13}Co_4$ and Al_5Co_2 is calculated based on Ref. [57].

Based on the step scanning measurements, relaxation is confirmed in this metallic glass, which has an impact on the crystallization. As evidenced by a similar $Ce_{68}Al_{10}Cu_{20}Fe_2$ metallic glass [39], crystallization mechanism can be changed with relaxation, where multiple crystallization peaks are detected consequently. However, the crystallization products are the same in that study, implying the negligible effect of relaxation on final phase formation. In the present experiment, however, the crystallization products are significantly distinguished, suggesting that the split of the crystallization peak is caused by both the relaxation and the ultrahigh heating rate. Since the composition of quasicrystals is totally different from the amorphous matrix, a primary crystallization is deemed to occur, which is evidenced by the first crystallization peak on DFSC heating curve. Furthermore, several kinds of ordered phases including some Ce-based crystals are detected after crystallization, implying a complicated crystallization behavior in this multicomponent metallic glass. A secondary crystallization is deemed to occur in this alloy, corresponding to the second crystallization peak in DFSC heating curve. On DSC heating (inset of Fig. 2), several minor exothermal peaks after the main crystallization are detected while they are absent on DFSC heating (Fig. 3a). Consistent with this argument, Al_5Co_2 that is identified on DSC heating is not observed in DFSC measurements. Since the quasicrystalline phase, $A1_{13}Co_4$, is thermodynamically metastable, it can evolve into stable Al_5Co_2 by reaction with undercooled liquid at elevated temperatures. On the ultrafast heating by DFSC, this transition may shift to temperature higher than 621 K, which is beyond the crystallization temperature range. In other words, the evolution from $Al_{13}Co_4$ to Al_5Co_2 is limited, leaving some undercooled liquid, corresponding to the mixed glassy-crystalline structure shown in Fig. 4.

In addition to the phase variations on DSC and DFSC crystallization, $Al_{13}Co_4$ quasicrystals exhibit apparent size discrepancy after rapid crystallization, as demonstrated in Fig. 4b. To shed light on the mechanism behind this phenomenon, HAADF-STEM mode in addition to bright-field image was employed to determine the Z-contrast regions, as pictured in Fig. 6a. Using EDS, composition fluctuations of Cu and Al are detected while Ce and Co are uniformly distributed after rapid crystallization [58]. Associated with the TEM image shown in Fig. 4a, area A with refined nanocrystals

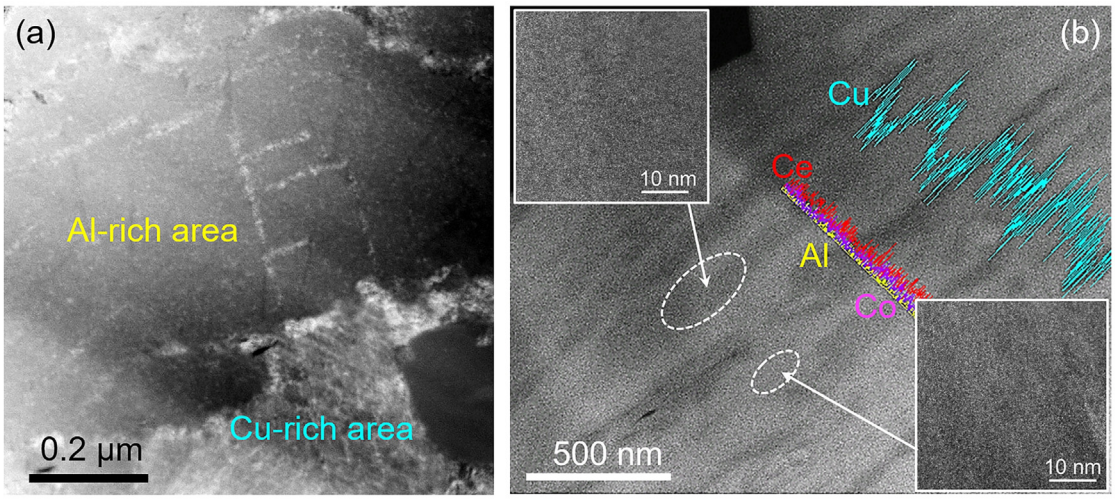

Fig. 6 – HAADF-STEM images of the (a) as-crystallized and (b) as-cast sample. Both Cu and Al segregate after crystallization, resulting in the contrasts in (a). In (b), only the segregation of Cu is detected while other elements are uniformly distributed. Insets in (b) are the high-resolution images for various areas, showing the amorphous structure.

is rich in Al element while Cu element is abundant in area *B* with coarse grains. As a comparison, Fig. 6b demonstrates the HAADF-STEM image of the as-cast BMG sample in which different contrasts are observed as well (more TEM images can be found in Fig. S3). In contrast to the as-crystallized sample, only a fluctuation of Cu element is observed in the fully amorphous regions. $Ce_{68}Al_{10}Cu_{20}Co_2$ BMG has a T_g close to room temperature, and it is therefore convincing that atoms begin to rearrange and diffuse just after casting [37], presumably resulting in the composition discrepancy. Consequently, both the nucleation and growth, which are central to the crystallization, are manifestly influenced on the following heating, and various crystallization behaviors are expected in different regions. For $Ce_{68}Al_{10}Cu_{20}Co_2$ system, Ce works as the matrix while Al and Cu are the main solute elements. Compared with Al, Cu atoms have a smaller radius, and a particular mobility is therefore achieved [59–61]. After casting and being stored at room temperature, Cu atoms can diffuse in the sample, inducing the composition heterogeneity in the amorphous matrix. For the atom pairs in $Ce_{68}Al_{10}Cu_{20}Co_2$ BMG, only Cu and Co displays a positive enthalpy of mixing (6 kJ/mol [61]). According to Inoue's criteria [62,63], this positive mixing enthalpy can reduce the glass forming ability and deteriorate the stability of the undercooled melt. It is therefore easier for the nucleation to occur in the Cu-rich region. Although some external factors such as heating rate [9] and pressure [64] can affect the crystallization behavior, the nucleation and growth rates are the intrinsic factors controlling the crystallization of metallic glass. For the particular case of quasicrystals, chemical short-rang order is especially important in their growth [65]. In Cu-rich region, the repulsive force between Co and Cu is larger, and an additional energy for Al–Co pair is thus produced as compared with Cu-poor zones. In other words, the growth for Al–Co is accelerated by Cu element in the Cu-rich region. It is therefore proposed that both the facilitated nucleation and enhanced growth contribute to the coarse crystals in the Cu-rich area.

4. Conclusions

Rapid crystallization of $Ce_{68}Al_{10}Cu_{20}Co_2$ BMG was realized by nanocalorimetry. When heated at 5000 K/s, the sample shows an altered crystallization behavior as compared with that crystallized at 10 K/min by conventional DSC, which digs out the initial stage of crystallization and depicts the trajectory of devitrification.

Multi-stage crystallization starting with the precipitation of $Al_{13}Co_4$ quasicrystals proceeds in $Ce_{68}Al_{10}Cu_{20}Co_2$ BMG. Working as the precursor on devitrification, this metastable phase bridges the structural gap between local atomic configurations in metallic glass and crystallization products. Co element plays the essential role in the nucleation of quasicrystals attributing to its covalent-like bond with Al.

Attributing to the particular mobility of Cu atoms, a composition redistribution is detected in the as-cast $Ce_{68}Al_{10}Cu_{20}Co_2$ BMG, which causes distinct crystallization behaviors in the different regions on the following heating. The enrichment of Cu destabilizes the undercooled melt and promotes the nucleation and growth of $Al_{13}Co_4$ quasicrystals on crystallization, resulting in the coarse crystals compared with Cu-poor regions.

The application of DFSC provides new insights into the devitrification of bulk metallic glasses, making it feasible to control and quantify phase transformations under extremely non-equilibrium conditions.

Conflicts of interest

The authors declare no conflicts of interest.

Acknowledgements

This work is supported by the National Natural Science Foundation of China (Grant Nos. 51671123, 51171105 and 50971086),

the Program for Professor of Special Appointment (Eastern Scholar) at Shanghai Institutions of Higher Learning (Grant No. TP2014042). BGZ thanks the support by China Postdoctoral Science Foundation (Grant No. 2018M640376). CS acknowledge financial support from the Ministry of Education and Science of the Russian Federation (Grant No. 14.Y26.31.0019).

Appendix A. Supplementary data

Supplementary data associated with this article can be found, in the online version, at doi:10.1016/j.jmrt.2019.05.023.

REFERENCES

[1] Jun WK, Willens RH, Duwez P. Non-crystalline structure in solidified gold–silicon alloys. Nature 1960;187:869–70.
[2] Kumar G, Desai A, Schroers J. Bulk metallic glass: the smaller the better. Adv Mater 2011;23:461–76.
[3] Matias TB, Asato GH, Ramasco BT, Botta WJ, Kiminami CS, Bolfarini C. Processing and characterization of amorphous magnesium based alloy for application in biomedical implants. J Mater Res Technol 2014;3:203–9.
[4] Tantavisut S, Lohwongwatana B, Khamkongkaeo A, Tanavalee A, Tangpornprasert P, Ittiravivong P. The novel toxic free titanium-based amorphous alloy for biomedical application. J Mater Res Technol 2018;7:248–53.
[5] Greer AL. New horizons for glass formation and stability. Nat Mater 2015;14:542–6.
[6] Schroers J, Masuhr A, Johnson WL, Busch R. Pronounced asymmetry in the crystallization behavior during constant heating and cooling of a bulk metallic glass-forming liquid. Phys Rev B 1999;60:11855–8.
[7] Chen Z, Zhang Y, Wang S, Zhang JY, Tao Q, Zhang P. Microstructure and mechanical properties of undercooled $Fe_{80}C_5Si_{10}B_5$ eutectic alloy. J Alloys Compd 2018;747:846–53.
[8] Schroers J, Wu Y, Busch R, Johnson WL. Transition from nucleation controlled to growth controlled crystallization in $Pd_{43}Ni_{10}Cu_{27}P_{20}$ melts. Acta Mater 2001;49:2773–81.
[9] Pogatscher S, Uggowitzer PJ, Löffler JF. *In-situ* probing of metallic glass formation and crystallization upon heating and cooling via fast differential scanning calorimetry. Appl Phys Lett 2014;104:251908.
[10] Wang S, Chen Z, Feng LC, Liu YY, Zhang P, He YZ, et al. Nano-phase formation accompanying phase separation in undercooled CoCrCuFeNi-3 at.% Sn high entropy alloy. Mater Charact 2018;144:516–21.
[11] Simon C, Gao J, Mao Y, Wilde G. Fast scanning calorimetric study of nucleation rates and nucleation transitions of Au–Sn alloys. Scr Mater 2017;139:13–6.
[12] Kündig AA, Ohnuma M, Ohkubo T, Hono K. Early crystallization stages in a Zr–Cu–Ni–Al–Ti metallic glass. Acta Mater 2005;53:2091–9.
[13] Pauly S, Gorantla S, Wang G, Kühn U, Eckert J. Transformation-mediated ductility in CuZr-based bulk metallic glasses. Nat Mater 2010;9:473–7.
[14] Schick C, Lexa D, Leibowitz L. Differential scanning calorimetry and differential thermal analysis. In: Kaufmann EN, editor. Characterization of materials. Hoboken, NJ, USA: John Wiley & Sons, Inc.; 2012. p. 483–94.
[15] Kurz W, Giovanola B, Trivedi R. Theory of microstructural development during rapid solidification. Acta Metall 1986;34:823–30.
[16] Minakov AA, Schick C. Ultrafast thermal processing and nanocalorimetry at heating and cooling rates up to 1 MK/s. Rev Sci Instrum 2007;78:073902.
[17] Gao Y, Zhao B, Vlassak JJ, Schick C. Nanocalorimetry: door opened for in situ material characterization under extreme non-equilibrium conditions. Prog Mater Sci 2019;104:53–137.
[18] Lai SL, Ramanath G, Allen LH, Infante P. Heat capacity measurements of Sn nanostructures using a thin-film differential scanning calorimeter with 0.2 nJ sensitivity. Appl Phys Lett 1997;70:43–5.
[19] Lee D, Vlassak JJ. Diffusion kinetics in binary CuZr and NiZr alloys in the super-cooled liquid and glass states studied by nanocalorimetry. Scr Mater 2019;165:73–7.
[20] Li L, Yang B, Zhao B, Abyzov AS, Schmelzer JWP, Schick C, et al. Rapid solidification behavior of nano-sized Sn droplets embedded in the Al matrix by nanocalorimetry. Mater Res Express 2014;1:045012.
[21] Orava J, Greer AL, Gholipour B, Hewak DW, Smith CE. Characterization of supercooled liquid $Ge_2Sb_2Te_5$ and its crystallization by ultrafast-heating calorimetry. Nat Mater 2012;11:279–83.
[22] Chen B, Momand J, Vermeulen PA, Kooi BJ. Crystallization kinetics of supercooled liquid Ge–Sb based on ultrafast calorimetry. Cryst Growth Des 2016;16:242–8.
[23] Weber H, Orava J, Kaban I, Pries J, Greer AL. Correlating ultrafast calorimetry, viscosity, and structural measurements in liquid GeTe and $Ge_{15}Te_{85}$. Phys Rev Mater 2018;2:093405.
[24] Lee D, Zhao B, Perim E, Zhang H, Gong P, Gao Y, et al. Crystallization behavior upon heating and cooling in $Cu_{50}Zr_{50}$ metallic glass thin films. Acta Mater 2016;121:68–77.
[25] Yang B, Schmelzer JWP, Zhao B, Gao Y, Schick C. Glass transition and primary crystallization of $Al_{86}Ni_6Y_{4.5}Co_2La_{1.5}$ metallic glass at heating rates spanning over six orders of magnitude. Scr Mater 2019;162:146–50.
[26] Zhao B, Yang B, Abyzov AS, Schmelzer JWP, Rodríguez-Viejo J, Zhai Q, et al. Beating homogeneous nucleation and tuning atomic ordering in glass-forming metals by nanocalorimetry. Nano Lett 2017;17:7751–60.
[27] Zhao B, Li L, Zhai Q, Gao Y. Formation of amorphous structure in Sn3.5Ag droplet by *in situ* fast scanning calorimetry controllable quenching. Appl Phys Lett 2013;103:131913.
[28] Swaminathan P, Grapes MD, Woll K, Barron SC, LaVan DA, Weihs TP. Studying exothermic reactions in the Ni-Al system at rapid heating rates using a nanocalorimeter. J Appl Phys 2013;113:143509.
[29] Molina-Ruiz M, Lopeandía AF, González-Silveira M, Anahory Y, Guihard M, Garcia G, et al. Formation of Pd_2Si on single-crystalline Si (1 0 0) at ultrafast heating rates: an *in-situ* analysis by nanocalorimetry. Appl Phys Lett 2013;102:143111.
[30] Pogatscher S, Leutenegger D, Schawe JEK, Uggowitzer PJ, Löffler JF. Solid–solid phase transitions via melting in metals. Nat Commun 2016;7:11113.
[31] Johnson WL, Kaltenboeck G, Demetriou MD, Schramm JP, Liu X, Samwer K, et al. Beating crystallization in glass-forming metals by millisecond heating and processing. Science 2011;332:828–33.
[32] Zhuravlev E, Schick C. Fast scanning power compensated differential scanning nano-calorimeter: 1. The device. Thermochim Acta 2010;505:1–13.
[33] Zhao B, Li L, Lu F, Zhai Q, Yang B, Schick C, et al. Phase transitions and nucleation mechanisms in metals studied by nanocalorimetry: a review. Thermochim Acta 2015;603:2–23.
[34] Gao Y, Zhuravlev E, Zou C, Yang B, Zhai Q, Schick C. Calorimetric measurements of undercooling in single micron sized SnAgCu particles in a wide range of cooling rates. Thermochim Acta 2009;482:1–7.

[35] Wu W, Zhang Q, Zhao B, Zhang L, Zhai Q, Gao Y. Solidification behavior of indium droplets embedded in aluminum by differential fast scanning calorimetry. J Therm Anal Calorim 2018;135:2995–3003.
[36] Yang B, Perepezko JH, Schmelzer JWP, Gao Y, Schick C. Dependence of crystal nucleation on prior liquid overheating by differential fast scanning calorimeter. J Chem Phys 2014;140:104513.
[37] Zhang B, Zhao DQ, Pan MX, Wang WH, Greer AL. Amorphous metallic plastic. Phys Rev Lett 2005;94:205502.
[38] Zhang B, Zhao DQ, Pan MX, Wang RJ, Wang WH. Formation of cerium-based bulk metallic glasses. Acta Mater 2006;54:3025–32.
[39] Luo Q, Zhang B, Zhao DQ, Wang RJ, Pan MX, Wang WH. Aging and stability of cerium-based bulk metallic glass. Appl Phys Lett 2006;88:151915.
[40] Bian Z, Inoue A. Ultra-low glass transition temperatures in Ce-based bulk metallic glasses. Mater Trans 2005;46:1857–60.
[41] Zhang B, Wang RJ, Zhao DQ, Pan MX, Wang WH. Superior glass-forming ability through microalloying in cerium-based alloys. Phys Rev B 2006;73:092201.
[42] Scherrer P. Bestimmung der Grösse und der inneren Struktur von Kolloidteilchen mittels Röntgenstrahlen. Nachr Ges Wiss 1918;26:98–100.
[43] Johari GP, Hallbrucker A, Mayer E. The glass–liquid transition of hyperquenched water. Nature 1987;330:552–3.
[44] Tkatch VI, Limanovskii AI, Kameneva VY. Studies of crystallization kinetics of $Fe_{40}Ni_{40P14}B_6$ and $Fe_{80}B_{20}$ metallic glasses under non-isothermal conditions. J Mater Sci 1997;32:5669–77.
[45] Okulov IV, Soldatov IV, Sarmanova MF, Kaban I, Gemming T, Edström K, et al. Flash Joule heating for ductilization of metallic glasses. Nat Commun 2015;6:7932.
[46] Farjas J, Roura P. Solid-phase crystallization under continuous heating: kinetic and microstructure scaling laws. J Mater Res 2008;23:418–26.
[47] Gerges J, Affouard F. Predictive calculation of the crystallization tendency of model pharmaceuticals in the supercooled state from molecular dynamics simulations. J Phys Chem B 2015;119:10768–83.
[48] Shneidman VA, Weinberg MC. Crystallization of rapidly heated amorphous solids. J Non-Cryst Solids 1996;194:145–54.
[49] Orava J, Greer AL. Kissinger method applied to the crystallization of glass-forming liquids: regimes revealed by ultra-fast-heating calorimetry. Thermochim Acta 2015;603:63–8.
[50] Addou R, Gaudry E, Deniozou Th, Heggen M, Feuerbacher M, Gille P, et al. Structure investigation of the (1 0 0) surface of the orthorhombic $Al_{13}Co_4$ crystal. Phys Rev B 2009;80:014203.
[51] Kandaskalov D, Fournée V, Ledieu J, Gaudry É. Adsorption properties of the o-$Al_{13}Co_4$ (1 0 0) surface toward molecules involved in the semihydrogenation of acetylene. J Phys Chem C 2014;118:23032–41.
[52] Xi X, Li LL, Zhang B, Wang W, Wu Y. Correlation of atomic cluster symmetry and glass-forming ability of metallic glass. Phys Rev Lett 2007;99:095501.
[53] Cheng YQ, Ma E. Atomic-level structure and structure-property relationship in metallic glasses. Prog Mater Sci 2011;56:379–473.
[54] Holland-Moritz D. Short-range order and solid–liquid interfaces in undercooled metallic melts. Mater Sci Eng A 2001;304-306:108–13.
[55] Han SW, Booth CH, Bauer ED, Huang PH, Chen YY, Lawrence JM. Lattice disorder and size-induced Kondo behavior in $CeAl_2$ and $CePt_{2+x}$. Phys Rev Lett 2006;97:097204.
[56] Gille P, Bauer B. Single crystal growth of $Al_{13}Co_4$ and $Al_{13}Fe_4$ from Al-rich solutions by the Czochralski method. Cryst Res Technol 2008;43:1161–7.
[57] Shevchenko MA, Berezutskii VV, Ivanov MI, Kudin VG, Sudavtsova VS. Thermodynamic properties of alloys of the Al–Co and Al–Co–Sc systems. Russ J Phys Chem 2014;88:729–34.
[58] Zhao B, Li L, Zhai Q, Gao Y. Structure characterization of Sn-based and Ce-based alloys treated by ultrafast scanning. In: Carpenter JS, Bai C, Hwang J-Y, Ikhmayies S, Li B, Monteiro SN, et al., editors. Characterization of minerals, metals, and materials. John Wiley & Sons, Inc.; 2014. p. 227–34.
[59] Angell CA, Ngai KL, McKenna GB, McMillan PF, Martin SW. Relaxation in glass forming liquids and amorphous solids. J Appl Phys 2000;88:3113–57.
[60] Evenson Z, Naleway SE, Wei S, Gross O, Kruzic JJ, Gallino I, et al. β relaxation and low-temperature aging in a Au-based bulk metallic glass: from elastic properties to atomic-scale structure. Phys Rev B 2014;89:174204.
[61] Takeuchi A, Inoue A. Classification of bulk metallic glasses by atomic size difference, heat of mixing and period of constituent elements and its application to characterization of the main alloying element. Mater Trans 2005;46:2817–29.
[62] Inoue A. Stabilization of supercooled liquid and opening-up of bulk glassy alloys. Proc Jpn Acad Ser B 1997;73:19–24.
[63] Inoue A. Stabilization of metallic supercooled liquid and bulk amorphous alloys. Acta Mater 2000;48:279–306.
[64] Zhang J, Wei YH, Qiu KQ, Zhang HF, Quan MX, Hua ZQ. Crystallization kinetics and pressure effect on crystallization of $Zr_{55}Al_{10}Ni_5Cu_{30}$ bulk metallic glass. Mater Sci Eng A 2003;357:386–91.
[65] Schroers J, Holland-Moritz D, Herlach DM, Urban K. Growth kinetics of quasicrystalline and polytetrahedral phases of Al–Pd–Mn, Al–Co, and Al–Fe from the undercooled melt. Phys Rev B 2000;61:14500–6.